Amazon Rainforest Mapping using Sentinel-1 Short Time Series

Andrea Pulella, Francescopaolo Sica, and Paola Rizzoli
Microwaves and Radar Institute, German Aerospace Center (DLR), Münchener Straße 20, 82234 Weßling (Germany)

Abstract

The present work aims at showing the application of Sentinel-1 *Short-Time-Series* for the constant monitoring of forests at large scale. In particular, here we present how the interferometric capabilities of the Sentinel-1 satellite constellation can be exploited for the monthly mapping of the Amazon rainforest. We model the interferometric coherence temporal trend as an exponential decay and retrieve interferometric parameters that are eventually exploited as input features to a Random Forests classifier.

1 Introduction

The Amazon is the world's largest tropical rainforest. Many are the reasons for its global importance: for example it contains the largest collection of animals and plants in the planet, it supports the life of millions of indigenous people, and it provides about 20% of the Earth's oxygen. Due to an increase in human population, in the last decades the Amazon region has been integrated into the global economy as one of the first sources of human feed and the pace of change at the edges of the forest has significantly accelerated. In order to monitor this precarious tendency, an up-to-date assessment of forest resources is of paramount importance and spaceborne Synthetic Aperture Radar (SAR) systems play a crucial role in providing consistent data, thanks to their unique property to provide a day-night global coverage in all weather conditions. Since 2014, global forest/non-forest classification maps derived from SAR data have been proposed, exploiting, for example, the sole backscatter of L-band sensor ALOS PALSAR in HV polarization [11] or the single-pass volume decorrelation coefficient of X-band bistatic TanDEM-X acquisitions [12]. In this paper we present the advances of an already assessed forest/non-forest classification algorithm [14] based on the use of repeat-pass interferometric acquisitions from the C-band Sentinel-1 constellation. The Sentinel-1 mission is designed to provide an operational interferometry capability through stringent requirements as the tight orbit control (orbital tube of 50m radius (rms)) and the short revisit time (6 days repeat-pass) [8] and operationally acquires data using the Interferometric Wide swath (IW) mode, with swath width of 260 km at a moderate resolution (5 m$\times$20 m). The paper is organized as follows: Sec. 2 introduces the proposed methodology for the generation of a forest/non-forest map, by applying a Random Forests classification algorithm [3]. Sec. 3 presents the materials used for the development of this work: the Sentinel-1 interferometric stacks and the external reference map over the selected site. In Sec. 4 the experimental results of the developed classification algorithm are described. Finally, Sec. 5 draws the conclusions and outlook.

2 Methodology

In this section the developed processing chain [15] is presented and it can be summarized by looking at the block diagram in Fig. 1.

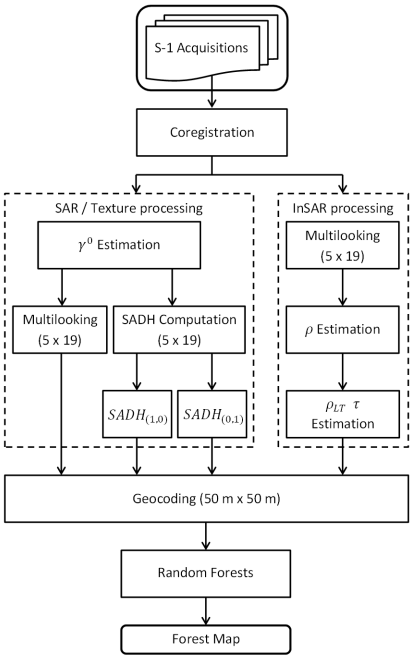

Figure 1 Sentinel-1 multi-temporal processing chain.

We consider a set of five repeat-pass acquisitions in VV polarization, which correspond to 30 days observation interval. According to Fig. 1, we coregister the images with respect to the master image, selected as the one at the center of the temporal stack. From the coregistered SAR images, we then retrieve parameters related to both backscatter and interferometric coherence. Indeed, the *SAR / Texture processing* branch of Fig. 1 depicts the procedure for the retrieval of the backscatter information. It consists of averaging along time all the backscatter projections, γ^0, each one associated to the relative acquisition in the stack.

The result is a multi-temporal backscatter parameter with a lower residual speckle, on which we can retrieve further textural information, by applying the Sum And Difference Histograms (SADH) method [1]. In particular, we can identify two set of textures, considering the spatial dependency among neighbouring pixels along azimuth and slant-range [15], reported in Figure 1 as $SADH_{(1,0)}$ and $SADH_{(0,1)}$, respectively. At the same time, the *InSAR processing* branch is dedicated to the estimation of temporal interferometric parameters, such as the temporal decorrelation constant and the long-term coherence [14]. We simultaneously exploit the whole interferometric stack to compute the coherence matrix and isolate the term that only depends from temporal decorrelation phenomena, by factorizing the coherence as presented in [14].

Assuming the local stationarity of the interferometric signal, the temporal decorrelation coefficient ρ_{temp} can be isolated from the interferometric coherence through a compensation for all other sources of decorrelation. Since the temporal decorrelation coefficients extracted from all the possible SLCs combinations describe the evolution in time of the coherence of a certain scatterer [5] and different scatterers decorrelate with different velocities, the evolution in time can be approximated as an exponential decay [5], [7] and in this paper we will show the results given by the following bi-parametric model, according to [14]:

$$\rho_{\text{temp}}(t) = (1 - \rho_{\text{LT}})\, e^{-\left(\frac{t}{\tau}\right)^2} + \rho_{\text{LT}}, \qquad (1)$$

where ρ_{LT} is the long term coherence and represents the residual temporal coherence of the target after a time much greater then the satellite revisit time T, while τ is the temporal decorrelation constant, a parameter that regulates the exponential decay. For the estimation of both parameters, a least square fitting is performed, considering as input points all the temporal decorrelation combinations. Thus, the last part of the processing chain in Fig. 1 is dedicated to the classification stage. The retrieved parameters estimated in the sub-chains, $\hat{\gamma_0}$, $SADH_{(1,0)}$, $SADH_{(0,1)}$, $\hat{\tau}$, and $\hat{\rho_{\text{LT}}}$, are then used as input features to a Random Forests machine learning classifier. Additionally, the local incidence angle θ_{inc} is also considered, since it merges the topography information (i.e. the Digital Elevation Model) and the acquisition geometry.

3 Materials

In order to assess the effectiveness of the proposed approach, a collection of 12 *Short-Time-Series*, covering the majority of the Rondonia state, Brazil, has been processed. In Fig. 2 we depict the reference map over the area of interest taken from the FROM-GLC-2017 dataset [13]. The observation interval chosen for this analysis is 30 days, the stack comprises 5 images at 6 days revisit time and is acquired between the end of April 2019 and the end of May 2019 (see Fig. 3). The description of the exploited dataset as well as the generated interferometric pairs is summarized in Tab. 1.

The classification results are compared with an external reference map, the FROM-GLC map [13]. This product

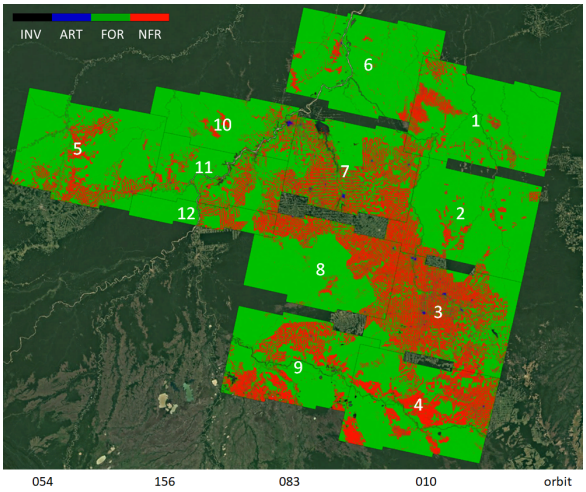

Figure 2 Finer Resolution Observation and Monitoring of Global Land Cover (FROM-GLC, 2017) reference chosen for the training and validation stages. Black: invalids (INV), Blue: artificial surfaces (ART), Green: forests (FOR), Red: non-forested areas (NFR).

is the result of a Random Forests classifier using as input parameters, several features extracted from Landsat Thematic Mapper (TM) and Enhanced Thematic Mapper Plus (ETM+) data, updated at 10 meters using an additional dataset of Sentinel-2 images acquired in 2017. Since this global land cover map comprises an inventory of 10 land cover classes, we grouped them into four macro-classes, according to [14]: artificial surfaces (ART), forests (FOR), non-forested areas (NFR), and water bodies and unclassified or no data as invalids (INV), as shown in Tab. 2.

4 Experimental Results

In the following, we show the experimental results obtained by applying the proposed methodology to the selected test site in the Amazon rainforest.

After generating the feature mentioned in Sec. 2, we select 5 million pixels for each of the considered classes for training the Random Forests algorithm. These samples are randomly selected from all the available dataset of Tab. 1, with the exception of the time series number 7, chosen for the validation step.

We present the results over four regions (here also indicated as *patches*), which are characterized by the presence of each of the considered classes. Indeed, as seen in Fig. 4, patches (a) and (b) are dominated by urban areas, Porto Velho and Ariquemes cities respectively, while patches (c) and (d) correspond to forest with clear-cuts areas.

Fig. 4 shows the classification maps obtained with our algorithm for the patches (a) to (d). Numerical results about the overall accuracy (OA) and the average accuracy (AA) are shown in Tab. 3. We notice from both visual inspection and numerical results that the algorithm is able to preserve the resolution of the data by retaining most of the details. In all patches we notice that the algorithm can distinguish very well between the forest (FOR) and non-forest (NFR)

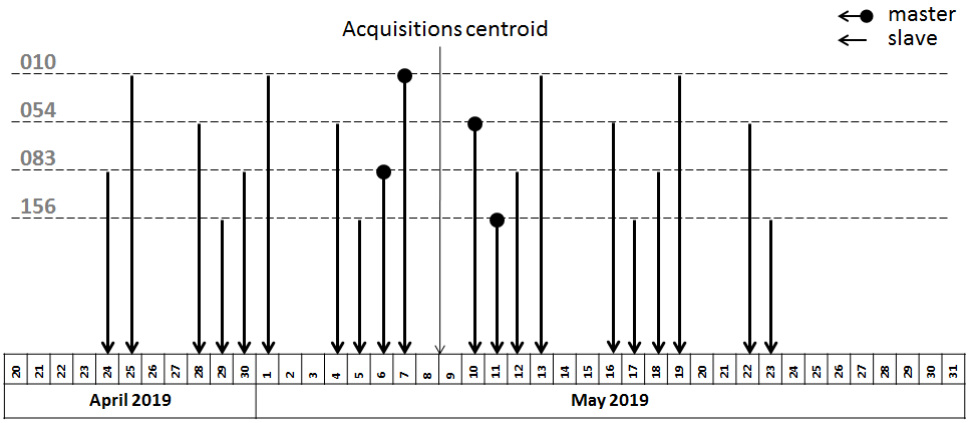

Figure 3 Sentinel-1 acquisitions time description. A dot represents the master image, while the arrows represent the date of the slave images.

			Corner Coordinates [deg]			
Stack	**Orbit**	**Name**	**Lat. min**	**Lat. max**	**Lon. min**	**Lon. max**
1	010	TS_0	$9°40'58.34"S$	$7°42'53.99"S$	$59°52'18.71"W$	$61°44'43.20"W$
2	010	TS_1	$11°16'36.74"S$	$9°15'31.41"S$	$60°12'59.94"W$	$62°5'1.52"W$
3	010	TS_2	$12°45'21.09"S$	$10°43'21.81"S$	$60°33'23.20"W$	$62°26'23.22"W$
4	010	TS_3	$14°10'32.67"S$	$12°12'43.74"S$	$60°53'48.14"W$	$62°46'54.92"W$
5	054	TS_0	$10°12'15.96"S$	$8°4'40.60"S$	$66°8'34.73"W$	$67°59'40.25"W$
6	083	TS_0	$8°51'9.51"S$	$6°50'56.20"S$	$61°42'32.10"W$	$63°36'0.35"W$
7	083	TS_1	$10°22'8.36"S$	$8°32'54.94"S$	$62°4'44.36"W$	$63°37'30.02"W$
8	083	TS_2	$11°51'16.77"S$	$10°2'26.15"S$	$62°25'15.09"W$	$64°19'5.05"W$
9	083	TS_3	$13°24'3.87"S$	$11°32'42.18"S$	$62°44'38.52"W$	$64°40'34.71"W$
10	156	TS_0	$9°24'34.67"S$	$8°4'15.76"S$	$63°53'30.37"W$	$65°56'1.88"W$
11	156	TS_1	$10°15'7.76"S$	$8°48'35.78"S$	$64°5'7.05"W$	$66°8'22.17"W$
12	156	TS_2	$10°36'21.14"S$	$9°46'22.31"S$	$64°9'39.68"W$	$66°19'6.56"W$

Table 1 Sentinel-1 stacks geographical position: relative orbit number, name of the time series associated to the orbit number, corner coordinates in latitude (lat.) and longitude (lon.).

Table 2 FROM-GLC classes aggregation strategy: artificial surfaces (ART), forests (FOR), non-forested areas (NFR), and water bodies and unclassified or no data as invalids (INV).

FROM-GLC	**Higher-level classes**
Unclassified	INV
Cropland	NFR
Forest	FOR
Grassland	NFR
Shrubland	NFR
Wetland	NFR
Water	INV
Tundra	NFR
Impervious surface	ART
Bareland	NFR
Snow/Ice	INV

classes, while the artifical surfaces (ART) are often misclassified as non-forest (patches (a) and (b)). The reason may be ascribed to the lower availability of ART samples in the training dataset. Indeed this class has hundred times less samples, that are recouped by replicating the available samples. This inconvenient can be avoided by considering larger datasets. On the other hand, the main goal of this work is forest mapping and a misclassification of ART classes is not of primary importance. Patches (c) and (d) show a higher agreement with the reference as also confirmed by the accuracy values. These two results are indeed a very good example of how we can distinguish between forested areas and clear-cuts. By repeating the classification on a monthly schedule, effectively monitoring the forest evolution in time.

Table 3 Overall accuracy (OA) and Average accuracy (AA) for the four patches in Fig. 4: (a) and (b) are characterized by urban areas, while (c) and (d) contain clear-cuts.

metric	**patch (a)**	**patch (b)**	**patch (c)**	**patch (d)**
OA	73.60%	82.49%	95.75%	87.98%
AA	78.15%	85.98%	94.28%	87.88%

5 Conclusions

In the present work we assess the performance of Sentinel-1 repeat-pass interferometry for forest classification over the Amazon rainforest. Experimental results confirm the

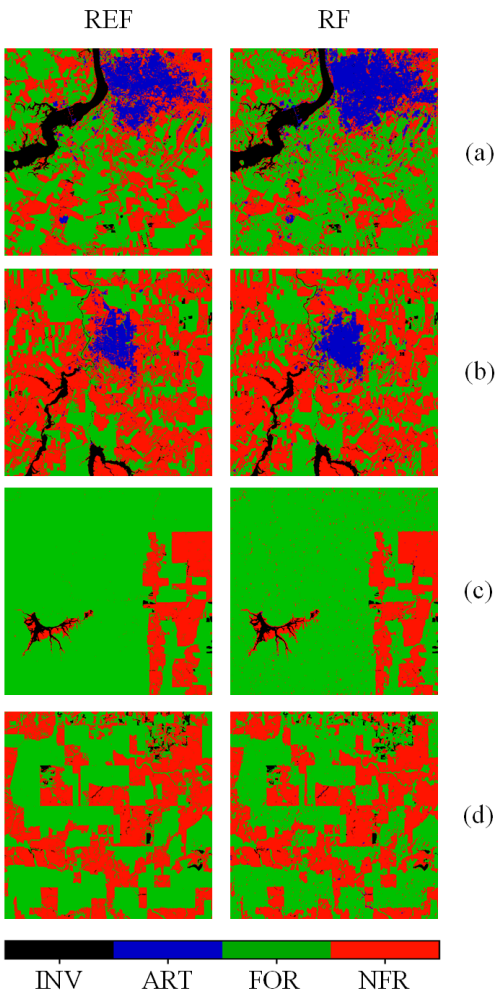

Figure 4 RF Classification map for four patches (a), (b), (c), (d) selected from the classification results over Stack number 7 in Tab. 1. REF is the Finer Resolution Observation and Monitoring of Global Land Cover (FROM-GLC, 2017) reference.

efficacy of this approach. Furthermore, the possibility of a monthly mapping allows for a constant monitoring over time of the Amazon rainforest. Future investigation will regard the analysis of the possible causes of misclassification and the implementation of further classification approaches.

6 Literature

[1] Unser, M. (1986), "Sum and difference histograms for texture classification", IEEE Transactions on Pattern Analysis and Machine Intelligence, vol. PAMI-8 (1), pp. 118–125.

[2] Zebker, H. A., and Villasenoir J. (1992). "Decorrelation in interferometric radar echoes", IEEE Transactions on geoscience and remote sensing, vol. 30 (5), pp. 950-959.

[3] Breiman, L. (2001). "Random forests", Machine Learning, vol. 45, pp. 5–32.

[4] Bruzzone, L., Marconcini, M., Wegmuller U., and Wiesmann A. (2004). "An Advanced System for the Automatic Classification of Multitemporal SAR Images", IEEE Transactions on Geoscience and Remote Sensing, vol. 42 (6), pp. 1321-1334.

[5] Rocca, F. (2007). "Modeling interferogram stacks", IEEE Transactions on Geoscience and Remote Sensing, vol. 45(10), pp. 3289-3299

[6] Krieger, G., Moreira, A., Fiedler, H., Hajnsek, I., Werner, M., Younis, M., and Zink, M. (2007). "TanDEM-X: A satellite formation for high-resolution SAR interferometry", IEEE Transactions on Geoscience and Remote Sensing, vol. 45 (11).

[7] Parizzi, A., Cong, X. Y., and Eineder, M. (2010). "First Results from Multifrequency Interferometry. A Comparison of Different Decorrelation Time Constants at L, C and X Band", ESA Special Publication, vol. 677.

[8] Torres, R., Snoeij, P., Geudtner, D., Bibby, D., Davidson, M., Attema, E., Potin, P., Rommen, B., Floury, N., Brown, M., Traver, I. N., Deghaye, P., Duesmann, B., Rosich, B., Miranda, N., Bruno, C., L'Abbate, M., Croci, R, Pietropaolo, A., Huchler, M., and Rostan, F. (2012). "GMES Sentinel-1 mission", Remote Sensing of Environment, vol. 120, pp. 9-24.

[9] Martone, M., Bräutigam, B., Rizzoli, P., Gonzalez, C., Bachmann, and M., Krieger, G. (2012). "Coherence evaluation of TanDEM-X interferometric data", ISPRS J. Photogramm. Remote Sens. vol. 73, pp. 21–29.

[10] Gong, P., J. Wang, L. Yu, Y. C. Zhao, Y. Y. Zhao, L. Liang, Z. G. Niu, et al. (2013). "Finer Resolution Observation and Monitoring of Global Land Cover: First Mapping Results with Landsat TM and ETM+ Data", International Journal of Remote Sensing, vol. 34 (7), pp. 2607-2654.

[11] Shimada, M., Itoh, T., Motooka, T., Watanabe, M., Shiraishi, T., Thapa, R., and Lucas, R. (2014). "New global forest/non-forest maps from ALOS PALSAR data (2007–2010)", Remote Sensing of Environment, vol. 155, pp. 13–31.

[12] Martone, M., Rizzoli, P., Wecklich, C., Gonzalez, C., Bueso-Bello, J. L., Valdo, P., Schulze, D., Zink, M., Krieger, G., and Moreira, A. (2018). "The Global Forest/Non-Forest Map from TanDEM-X Interferometric SAR Data", Remote Sensing of Environment, vol. 205, pp. 352-373.

[13] Gong P., Liu H., Zhang M., et al. (2019). "Stable classification with limited sample: transferring a 30-m resolution sample set collected in 2015 to mapping 10-m resolution global land cover in 2017", Science Bulletin, vol. 64 (6), pp. 370-373.

[14] Sica, F., Pulella, A., Nannini, M., Pinheiro, M., and Rizzoli, P. (2019). "Repeat-pass SAR interferometry for land cover classification: A methodology using Sentinel-1 Short-Time-Series", Remote Sensing of Environment, vol. 232 (111277).

[15] Pulella, A., Santos, R., Sica, F., Posovszky., P., and Rizzoli, P. (2020). "Multi-Temporal Sentinel-1 Backscatter and Coherence for Rainforest Mapping", Remote Sensing, vol. 12 (847).